A numerical analysis of an anisotropic phase-field model for binary-fluid mixtures in the presence of magnetic-field

Aziz Belmiloudi, Amer Rasheed

A numerical analysis of an anisotropic phase-field model for binary-fluid mixtures in the presence of magnetic-field

A. Belmiloudi*, A. Rasheed†

Abstract

In this paper we propose a numerical scheme and perform its numerical analysis devoted to an anisotropic phase-field model with convection under the influence of magnetic field for the isothermal solidification of binary mixtures in two-dimensional geometry. Precisely, the numerical stability and error analysis of this approximation scheme which is based on mixed finite-element method are performed. The particular application of a nickelcopper (NiCu) binary alloy, with real physical parameters, is considered. The study substantiates a good agreement between the numerical and theoretical results, and demonstrates the efficiency of the presented method.

keyword Mixed finite elements, stability and error analysis, anisotropic phase-field, dendritic solidification, binary alloys, fluid flow, magnetic-field.

1 Introduction

The understanding and control over the evolution of dendrites during the solidification process of metals and alloys has a critical impact on the final solidified material. The voracious investigators have, therefore, performed a great deal of experimental as well as mathematical and numerical studies to explore the microstructure in alloys. In recent years phase field models have become an important tool to simulate, during the solidification process of pure and mixtures of materials, the formation and growth of dendrites. This paradigm allowed several investigators to understand and analyze the peculiarities of the synthesis and dynamics of materials during the past couple of decades, see for instance [1, 4, 8, 13, 14, 15, 25, 27, 28, 29] and the references therein. In order to ameliorate the quality of the final solidified metal in the industrial processes, it is essential to control the evolution of dendrites during the solidification process, albeit these models are unable to render control over dendrite growth and micro-segregation stand-alone. Nevertheless, experimental studies indicate that the control can be procured in the solidification process by virtue of applied external electric and magnetic fields see e.g. [12, 22] and the references therein. For other applications of the influence of magnetic fields on the materials, we can cite, e.g., for the MHD flows Hadid et al. [10], for the semi-conductor melt flow in the crystal growth Belmiloudi [5], Gunzberger et al. [9], Watanabe et al. [30], Galindo et al. [7] and for the solidification processes, Roplekar and Dantzig [21], Prescott [22], Sampath [23] and the references therein.

In view of these facts, Rasheed and Belmiloudi in [18] (see also [16, 17, 20]) developed a phase-field model taking care of convection as well as magnetic field. Primarily, the two dimensional model of Warren-Boettinger [29] is considered and then, among other, the effect of convection in the phase-field and solute equations, and melt-flow equations in the presence of an externally applied magnetic field are included. The model is composed of three systems, the magnetohydrodynamic system which is obtained with the help of incompressible Navier-Stokes equations by using the Lorentz force and boussinesq approximations, the phase-field system and the concentration system. The phase field and concentration systems are the convection diffusion type systems which represent the phase change and relative concentration of the binary mixture during the solidification process. We refer the reader to [18] for detailed description of the model.

*Mathematics Research Institute of Rennes (IRMAR), European University of Brittany, INSA, 20 Av. Buttes de Coesmes, CS70839, 35708 Rennes Cedex7, France, aziz.belmiloudi@math.cnrs.fr

†Department of Mathematics, Lahore University of Management Sciences, Opposite Sector U, DHA,Lahore Cantt 54792, Pakistan, amerasheed@ciitwah.edu.pk,

In order to extend further our studies associated with dendritic growth in the binary alloys under the action of magnetic field using the phase field model proposed by Rasheed and Belmiloudi, it is indispensable to develop stable and effective numerical schemes able to carry out the realistic physical simulations. The purpose of this paper is then to provide a numerical approximation scheme based on mixed finite-element method, and numerical error and stability analysis for Rasheed and Belmiloudi model in the anisotropic case. Some numerical results in the isotropic case are presented in the note [19].

The organization of the paper is as follows. In the next section we recall briefly the mathematical model and we describe its weak formulation. Section 4 is dedicated to the discrete variational formulation, in the context of a mixed method. The stability of the discrete variational formulations is studied, and error estimates of the finite element approximations are performed and confirmed by numerical experiments in section 5. Finally, numerical simulations of the evolution of dendrites during the solidification of the binary mixture of Nickel-Copper (Ni-Cu) are presented in section 6.

2 Mathematical formulation

Initially a region Ω is occupied by a binary alloy composed by two pure elements, the solute B (e.g., Cu) and the solvent A (e.g., Ni), which is considered as incompressible electrically conducting fluid. To treat the system which represents the isothermal and anisotropic solidification process, we have considered the following phase field model for dendrite solidification due to Rasheed and Belmiloudi [18]. Let $\mathbf{u}$, p, ψ, c and $\mathbf{B}$ represent the velocity, pressure, phase, concentration and applied magnetic fields respectively. Then, in the absence of phase and concentration exchange across, and negligible melt velocity along $\partial\Omega$, we have the following system

$$\begin{cases} \rho_0\big(\partial_t\mathbf{u} + (\mathbf{u}\cdot\nabla)\mathbf{u}\big) = -\nabla p + \mu\Delta\mathbf{u} + \boldsymbol{\mathcal{A}}_1(\psi, c) + b(\psi)\big(\big(\mathbf{u}\times\mathbf{B}\big)\times\mathbf{B}\big) & \text{on } \mathcal{Q}, \\ \mathrm{div}\mathbf{u} = 0 & \text{on } \mathcal{Q}, \\ \partial_t\psi + (\mathbf{u}\cdot\nabla)\psi = \mathrm{div}\,(\mathcal{A}_{\mathrm{g}}(\nabla\psi)\nabla\psi) - \mathcal{A}_2(\psi, \mathrm{c}) & \text{on } \mathcal{Q}, \\ \partial_t c + (\mathbf{u}\cdot\nabla)c = \mathrm{div}\,(\mathrm{D}(\psi)\nabla\mathrm{c} + \mathcal{A}_3(\psi, \mathrm{c})\nabla\psi) & \text{on } \mathcal{Q}, \\ \text{subject to the initial conditions} & \\ (\mathbf{u}, \psi, c)\,(t=0) = (\mathbf{u}_0, \psi_0, c_0) & \text{on } \Omega, \\ \text{and the boundary conditions} & \\ \mathbf{u} = 0, \quad \mathcal{A}_g(\nabla\psi)\nabla\psi\cdot\mathbf{n} = 0, \quad (D(\psi)\nabla c + \mathcal{A}_3(\psi, c)\nabla\psi)\cdot\mathbf{n} = 0 & \text{on } \Sigma, \end{cases} \tag{2.1}$$

where $\Omega \subset \Re^2$ is a sufficiently smooth open solidification domain with regular boundary $\partial\Omega$, T is the final time of the solidification process, $\mathcal{Q} = \Omega\times(0,T)$, $\Sigma = \partial\Omega\times(0,T)$, $\rho_0 = \frac{\rho_0^{(A)}+\rho_0^{(B)}}{2}$ and $\mu = \frac{\mu^{(A)}+\mu^{(B)}}{2}$ are the average density and viscosity, $D(\psi)$ is the diffusion coefficient and $\mathbf{n}$ is the unit outward normal to $\partial\Omega$. The anisotropy matrix $\mathcal{A}_g$ is defined by

$$\mathcal{A}_g(\nabla\psi) = M_\psi \begin{pmatrix} \eta_\gamma^2(\theta) & -\eta_\gamma(\theta)\eta_\gamma'(\theta) \\ \eta_\gamma(\theta)\eta_\gamma'(\theta) & \eta_\gamma^2(\theta) \end{pmatrix}$$

where $M_\psi > 0$ is the interfacial mobility parameter and η_γ is the anisotropy function defined as [29]

$$\eta_\gamma = \epsilon_0(1 + \gamma\cos(k\theta)), \tag{2.2}$$

$\gamma \geq 0$ is the anisotropic amplitude, the integer $k > 1$ corresponds to the number of branching directions, ϵ_0 is a constant and θ (the angle between the x-axis and $\nabla\psi$)

$$\theta = \arctan\left(\frac{\psi_y}{\psi_x}\right), \tag{2.3}$$

is the angle between the local interface normal and a designated base vector of the crystal lattice, subscripts x and y are used to denote the partial derivatives with respect to spatial coordinates, that is $\psi_x = \partial\psi/\partial x$ and $\psi_y = \partial\psi/\partial y$. For low to moderate accuracy, $\gamma > 0$ is chosen so that the condition $\eta_\gamma(\theta) + \dfrac{d^2\eta_\gamma}{d\theta^2}(\theta) > 0$

is valid for all θ. For $k = 4$ (fourfold anisotropy) which is a case of physical relevance, the previous condition is valid iff $\gamma < \frac{1}{15} \approx 0,6667$. The operators $\boldsymbol{\mathcal{A}_1}$, $\mathcal{A}_2$ and $\mathcal{A}_3$ are defined by

$$\begin{aligned} &\boldsymbol{\mathcal{A}_1}(\psi, c) = \beta_c a_1(\psi) c\mathbf{G} + \zeta \mathbf{f}(\psi), \quad \mathcal{A}_2(\psi, c) = M_\psi(\frac{\lambda_1(c)}{\delta^2} g'(\psi) + \frac{\lambda_2(c)}{\delta}\bar{p}'(\psi)), \\ &\mathcal{A}_3(\psi, c) = \alpha_0 D(\psi) c(1-c)\left(\frac{\lambda_1'(c)}{\delta} g'(\psi) - \lambda_2'(c)\bar{p}'(\psi)\right), \end{aligned} \tag{2.4}$$

and function b by $b(\psi) = \sigma_e a_2(\psi)$ where *prime* denotes the ordinary derivative with respect to variable involved, $\sigma_e = \frac{\sigma_e^{(A)} + \sigma_e^{(B)}}{2}$ is the the average electric conductivity, $\mathbf{G}$ is the gravity vector, β_c is the solutal expansion coefficient, δ is the interface thickness, α_0 is a material parameter, λ_i $(i = 1, 2)$ are linear functions involving material dependent constants and, g, $\bar{p}$, a_1 and a_2 are included for modeling convenience satisfying the conditions $g(0) = g(1) = 0$, $g'(\psi) = 0$ iff $\psi \in \{0, 1, 1/2\}$, $g''(0), g''(1) > 0$, $g(\psi) = g(1-\psi)$, $\bar{p}(0) = \bar{p}(1) = 0$, $\bar{p}'(\psi) > 0$ for all $\psi \in (0, 1)$ and $a_i(0) = 0$ $(i = 1, 2)$. Throughout in this study, we assume $a_i(\psi) = \psi$, $\mathbf{f}(\psi) = (\psi, \psi)$, $\bar{p}(\psi) = \psi^3(10 - 15\psi + 6\psi^2)$ and $g(\psi) = \bar{p}'(\psi)/30$. For a complete description of the mathematical modeling, the reader is referred to [18].

Remark 2.1 *Note that to derive equations for the melt flow, we have assumed the Boussinesq approximations (see e.g. [3]), as is often done in the heat and/or solute transfer problems. This has led us to neglect the density variations with respect to temperature and/or concentration everywhere except in the gravitational force term in the momentum equation, and also neglecting the temperature variations of the other material properties. Also as we know that the phase-field variable ψ is 0 in the solid phase and 1 in the liquid phase and there is no motion in the solid phase, therefore equations of the melt flow should give us the zero velocity in the solid region of the domain. To include this fact in the equations of melt flow, we have multiplied the Boussinesq approximation term and Lorentz force term by functions $a_1(\psi)$ and $a_2(\psi)$. These functions are chosen in way that they are null at $\psi = 0$, so that the Boussinesq approximation term and Lorentz force term become zero in the solid region and the equations of the melt flow together with the zero initial and boundary conditions give the zero velocity in the solid region of the domain. Also to include the effects on the velocity with respect to the phase change at the solid/liquid interface, we have added an additional term $\mathbf{f}(\psi)$ in the flow equations which will also be chosen so that it is zero at $\psi = 0$ (it depends on the choice of the temperature).*

3 Weak formulation

We shall define some notations and basic spaces. The inner product and the norm in $L^2(\Omega)$ are respectively denoted by $(.,.)$ and $|\ .\ |$. We introduce the following spaces:

$$\begin{aligned} &\mathcal{W} = (H_0^1(\Omega))^2 = \left\{\mathbf{v} \in \ \left(H^1(\Omega)\right)^2 \ \mid \mathbf{v} = 0 \text{ on } \partial\Omega\right\}, \quad \mathcal{W}_d = \{\mathbf{v} \in \ \mathcal{W} \mid \text{div}(\mathbf{v}) = 0\ \}, \\ &\mathcal{M} = H^1(\Omega), \quad \mathcal{H} = \left\{q \in L^2(\Omega) \ \mid \int_\Omega q d\mathbf{x} = 0\right\}, \end{aligned} \tag{3.1}$$

where $\mathcal{W}$ is equipped with the norm $\|\ \nabla.\ \|$. The scalar product and norm in $\mathcal{H}$ are denoted by the usual $L^2(\Omega)$ inner product and its norm $(.,.)$ and $|\ .\ |$, respectively.

Remark 3.1 *: The condition $\int_\Omega q d\boldsymbol{x} = 0$ on the pressure is imposed in order to assure the uniqueness of the pressure because the pressure is defined within a class of equivalence, regardless of a time-dependent function. We can impose also other conditions on the pressure, in accordance on its regularity, e.g., the pressure is zero on part of the boundary, etc.*

Now, we define the following bilinear and trilinear forms as follows (for all $(\mathbf{u},\mathbf{v},\mathbf{w}) \in (\mathcal{W})^3$, $p \in \mathcal{H}$, $(c,z) \in (\mathcal{M})^2$ and $(\phi,\psi) \in (\mathcal{M})^2$):

$$a_u(\mathbf{u},\mathbf{v}) = \mu \int_\Omega \nabla\mathbf{u}\cdot\nabla\mathbf{v}d\mathbf{x}, \quad c_p(\mathbf{u},p) = -(\mathrm{div}(\mathbf{u}),\mathrm{p}), \quad b_u(\mathbf{u},\mathbf{v},\mathbf{w}) = \rho_0 \sum_{i,j=1}^{2} \int_\Omega u_i(\partial_i v_j) w_j d\mathbf{x},$$
$$b_c(\mathbf{u},c,z) = \sum_{i=1}^{2} \int_\Omega u_i(\partial_i c) z d\mathbf{x}, \quad b_\psi(\mathbf{u},\psi,\phi) = \sum_{i=1}^{2} \int_\Omega u_i(\partial_i \psi)\phi d\mathbf{x}.$$

Moreover, if $\mathrm{div}(\mathbf{u}) = 0$, the trilinear forms satisfy the classical relations given in the following Lemma (see e.g. [3, 26]):

Lemma 3.1 *The trilinear forms b_u, b_ψ, b_c have the following properties*

(i) For all $\boldsymbol{u} \in \mathcal{W}_d$, $\boldsymbol{v} \in \mathcal{W}$ and $\psi, c \in \mathcal{M}$

$$b_u(\boldsymbol{u},\boldsymbol{v},\boldsymbol{v}) = 0, \quad b_\psi(\boldsymbol{u},\psi,\psi) = 0, \quad b_c(\boldsymbol{u},c,c) = 0.$$

(ii) For all $\boldsymbol{u} \in \mathcal{W}_d$, $\boldsymbol{v},\boldsymbol{w} \in \mathcal{W}$ and $\psi,\phi,c,z \in \mathcal{M}$

$$b_u(\boldsymbol{u},\boldsymbol{v},\boldsymbol{w}) = -b_u(\boldsymbol{u},\boldsymbol{w},\boldsymbol{v}), \quad b_\psi(\boldsymbol{u},\psi,\phi) = -b_\psi(\boldsymbol{u},\phi,\psi), \quad b_c(\boldsymbol{u},c,z) = -b_c(\boldsymbol{u},z,c).$$

Multiplying the first and second equations of (2.1) by $\mathbf{v} \in \mathcal{W}$, third equation of (2.1) by $\phi \in \mathcal{M}$ and last equation of (2.1) by $z \in \mathcal{M}$, integrate the results over Ω with use of Green's formulas and use boundary conditions, we obtain the following weak formulation of the problem (2.1) (wherein we use artificial source terms $\mathbf{F}_u$, F_ψ and F_c for fabricating exact solutions thereby analyzing the convergence and stability of the numerical scheme): Find $(\mathbf{u},p,\psi,c) \in \mathcal{W}\times\mathcal{H}\times\mathcal{M}\times\mathcal{M}$ such that $\forall\ (\mathbf{v},q,\varphi,z) \in \mathcal{W}\times\mathcal{H}\times\mathcal{M}\times\mathcal{M}$

$$\begin{cases} \rho_0(\partial_t\mathbf{u},\mathbf{v}) + a_u(\mathbf{u},\mathbf{v}) + b_u(\mathbf{u},\mathbf{u},\mathbf{v}) + c_p(\mathbf{v},p) - (\boldsymbol{\mathcal{A}}_1(\psi,c),\mathbf{v}) \\ \qquad\qquad - (b(\psi)((\mathbf{u}\times\mathbf{B})\times\mathbf{B}),\mathbf{v}) = (\mathbf{F}_u,\mathbf{v}), \\ -c_p(\mathbf{u},q) = 0, \\ (\partial_t\psi,\varphi) + b_\psi(\mathbf{u},\psi,\varphi) + (\mathcal{A}_g(\nabla\psi)\nabla\psi,\nabla\varphi) + (\mathcal{A}_2(\psi,c),\varphi) = (F_\psi,\varphi), \\ (\partial_t c,z) + b_c(\mathbf{u},c,z) + (D(\psi)\nabla c,\nabla z) + (\mathcal{A}_3(\psi,c)\nabla\psi,\nabla z) = (F_c,z), \\ (\mathbf{u},\psi,c)(t=0) = (\mathbf{u}_0,\psi_0,c_0). \end{cases} \tag{3.2}$$

4 Discrete weak formulation and finite element discretization

Let $\mathcal{T}_h$ be a family of shape-regular triangulations of the domain $\overline{\Omega}$ with maximum mesh spacing parameter $0 < h = \max_{\mho\in\mathcal{T}_h} diam(\mho) < h_0 < 1$. To construct a Galerkin approximation of (3.2), we consider the $\mathbb{P}_l$, $\mathbb{P}_{l-1}$ and $\mathbb{P}_l$ finite element subspaces $\mathcal{W}_h$, $\mathcal{H}_h$ and $\mathcal{M}_h$ of $\mathcal{W}$, $\mathcal{H}$ and $\mathcal{M}$ respectively over the partition $\mathcal{T}_h$, where the polynomials $\mathbb{P}_l$ is the space of polynomials of degree at most l. Furthermore, we make the following assumptions $(\mathcal{H})$

(C1) $\exists\ c_1 > 0$, such that $\forall \mathbf{X} = (\mathbf{u},\psi,c) \in \left(H^{r+1}(\Omega)\right)^4 \cap \left(\mathcal{W}\times\mathcal{M}^2\right)$ and $\forall r \in [1,l]$

$$\inf_{\mathbf{X}_h\in\mathcal{W}_h\times\mathcal{M}_h^2} \|\mathbf{X}-\mathbf{X}_h\| \ \le\ c_1 h^r \|\mathbf{X}\|_{H^{r+1}(\Omega)}.$$

(C2) $\exists\ c_2 > 0$, such that $\forall\ q \in H^r(\Omega)\cap\mathcal{H}$ and $\forall\ r \in [1,l]$

$$\inf_{q_h\in\mathcal{H}_h} \|q-q_h\| \ \le\ c_2 h^r \|q\|_{H^r(\Omega)}.$$

(C3) $\exists\ c_3 > 0$ such that (Inf-Sup condition)

$$\inf_{q_h\in\mathcal{H}_h} \sup_{\mathbf{v}_h\in\mathcal{W}_h} \frac{c_p(\mathbf{v}_h,q_h)}{\|\mathbf{v}_h\|\,|q_h|} \ \ge\ c_3.$$

(C4) Let $\mathbf{X}_0 = (\mathbf{u}_0, \psi_0, c_0) \in \left(H^{r+1}(\Omega)\right)^4$ with $r \in [1, l]$, then

$$h \left\| \mathbf{X}_0 - \mathbf{X}_{0h} \right\| + \left| \mathbf{X}_0 - \mathbf{X}_{0h} \right| \ \leq \ c_4 h^{r+1},$$

where $\mathbf{X}_{0h} = (\mathbf{u}_{0h}, \psi_{0h}, c_{0h}) \in \mathcal{W}_h \times \mathcal{M}_h^2$ is the approximation of $\mathbf{X}_0$.

(C5) For all integers $\mathfrak{m}, \mathfrak{p}, \mathfrak{q}$ and $\mathfrak{k}$ with $0 < \mathfrak{p}, \mathfrak{q} \leq \infty$ and $\forall\ K \in \mathcal{T}_h$, we have

$$\begin{aligned} \left\| \mathbf{X}_h \right\|_{W^{\mathfrak{m},\mathfrak{q}}(K)} \ &\leq \ c_4\ h^{n/\mathfrak{q} - n/\mathfrak{p} + \mathfrak{k} - \mathfrak{m}}\ \left\| \mathbf{X}_h \right\|_{W^{\mathfrak{k},\mathfrak{p}}(K)}, \quad \forall\ \mathbf{X}_h \in \mathcal{W}_h \times \mathcal{M}_h^2, \\ \left\| \mathbf{X}_h \right\|_{W^{\mathfrak{m},\mathfrak{q}}(\Omega)} \ &\leq \ c_4\ h^{n/\mathfrak{q} - n/\mathfrak{p} + \mathfrak{k} - \mathfrak{m}}\ \left\| \mathbf{X}_h \right\|_{W^{\mathfrak{k},\mathfrak{p}}(\Omega)}, \quad \forall\ \mathbf{X}_h \in \mathcal{W}_h \times \mathcal{M}_h^2. \end{aligned}$$

We can now define the space and time discretization of the problem (3.2) i.e. the discrete weak formulation of the problem (2.1). We shall explain in detail the numerical scheme and give the space discretization and the general form of the differential-algebraic systems for (3.2). Then we present briefly the time discretization of the problem. For the discretization of the problem with respect to spatial coordinates, we have utilized mixed finite elements, which satisfy the Inf-Sup condition (Babuska-Brezi's condition), for the velocity $\mathbf{u}$ and pressure p and usual finite elements for phase-field ψ and concentration c state variables. The discrete weak formulation can be formulate as follows: Find $(\mathbf{u}_h, p_h, \psi_h, c_h) \in \mathcal{W}_h \times \mathcal{H}_h \times \mathcal{M}_h \times \mathcal{M}_h$ such that $\forall (\mathbf{v}_h, q_h, \varphi_h, z_h) \in \mathcal{W}_h \times \mathcal{H}_h \times \mathcal{M}_h \times \mathcal{M}_h$

$$\left\{ \begin{array}{l} \rho_0 \left(\partial_t \mathbf{u}_h, \mathbf{v}_h\right) + a_u \left(\mathbf{u}_h, \mathbf{v}_h\right) + b_u \left(\mathbf{u}_h, \mathbf{u}_h, \mathbf{v}_h\right) + c_p \left(\mathbf{v}_h, p_h\right) - \left(\boldsymbol{\mathcal{A}}_1(\psi_h, c_h), \mathbf{v}_h\right) \\ \qquad\qquad - \left(b(\psi_h)((\mathbf{u}_h \times \mathbf{B}) \times \mathbf{B}), \mathbf{v}_h\right) = \left(\mathbf{F}_u, \mathbf{v}_h\right), \\ -c_p \left(\mathbf{u}_h, q_h\right) = 0, \\ \left(\partial_t \psi_h, \varphi_h\right) + b_\psi(\mathbf{u}_h, \psi_h, \varphi_h) + \left(\mathcal{A}_g(\nabla\psi_h)\nabla\psi_h, \nabla\varphi_h\right) + \left(\mathcal{A}_2(\psi_h, c_h), \varphi_h\right) = \left(F_\psi, \varphi_h\right), \\ \left(\partial_t c_h, z_h\right) + b_c \left(\mathbf{u}_h, c_h, z_h\right) + \left(D(\psi_h)\nabla c_h, \nabla z_h\right) + \left(\mathcal{A}_3(\psi_h, c_h)\nabla\psi_h, \nabla z_h\right) = \left(F_c, z_h\right), \\ \left(\mathbf{u}_h, \psi_h, c_h\right)(t = 0) = \left(\mathbf{u}_{0h}, \psi_{0h}, c_{0h}\right). \end{array} \right. \tag{4.1}$$

Let $(\varphi_{ih})_{1 \leq i \leq M}$, $(q_{ih})_{2M+1 \leq i \leq 2M+N}$ and $(z_{ih})_{2M+N+1 \leq i \leq 2M+N+\tilde{M}}$ be the basis of $\mathcal{W}_h$, $\mathcal{H}_h$ and $\mathcal{M}_h$ respectively and

$$\begin{aligned} \mathbf{u}_h(x,t) &= \sum_{i=1}^{M} \mathbf{u}_{ih}(t)\varphi_{ih}(x) = \sum_{i=1}^{M} u_{ih}(t)\underline{\varphi}^u_{ih}(x) + \sum_{i=1}^{M} v_{ih}(t)\underline{\varphi}^v_{ih}(x), \qquad p_h(x,t) = \sum_{i=2M+1}^{2M+N} p_{ih}(t) q_{ih}(x), \\ \psi_h(x,t) &= \sum_{i=2M+N+1}^{2M+N+\tilde{M}} \psi_{ih}(t) z_{ih}(x), \qquad c_h(x,t) = \sum_{i=2M+N+\tilde{M}+1}^{2M+N+2\tilde{M}} c_{ih}(t) z_{ih}(x), \end{aligned} \tag{4.2}$$

where $\mathbf{u}_{ih} = \begin{pmatrix} u_{ih} \\ v_{ih} \end{pmatrix}$, $\underline{\varphi}^u_{ih} = \begin{pmatrix} \varphi_{ih} \\ 0 \end{pmatrix}$, $\underline{\varphi}^v_{ih} = \begin{pmatrix} 0 \\ \varphi_{ih} \end{pmatrix}$.

By virtue of (4.2), the semi-discrete weak form (4.1) yields

$$\begin{aligned}
&\sum_{i=1}^{M}\rho_0\left(\underline{\varphi}^u_{ih},\underline{\varphi}^u_{jh}\right)\frac{du_{ih}}{dt}+\sum_{i=1}^{M}\Big(a_u\left(\underline{\varphi}^u_{ih},\underline{\varphi}^u_{jh}\right)+b_u\left(\mathbf{u}_h,\underline{\varphi}^u_{ih},\underline{\varphi}^u_{jh}\right)\\
&\qquad-\left(b(\psi_h)((\underline{\varphi}^u_{ih}\times\mathbf{B})\times\mathbf{B}),\underline{\varphi}^u_{jh}\right)\Big)u_{ih}+\sum_{i=2M+1}^{2M+N}\left(q_{ih},div(\underline{\varphi}^u_{jh})\right)p_{ih}\\
&\qquad-\left(\boldsymbol{\mathcal{A}}_1(\psi_h,c_h),\underline{\varphi}^u_{jh}\right)+\sum_{i=1}^{M}\rho_0\left(\underline{\varphi}^v_{ih},\underline{\varphi}^v_{jh}\right)\frac{dv_{ih}}{dt}\\
&\qquad+\sum_{i=1}^{M}\Big(a_u\left(\underline{\varphi}^v_{ih},\underline{\varphi}^v_{jh}\right)+b_u\left(\mathbf{u}_h,\underline{\varphi}^v_{ih},\underline{\varphi}^v_{jh}\right)\\
&\qquad-\left(b(\psi_h)((\underline{\varphi}^v_{ih}\times\mathbf{B})\times\mathbf{B}),\underline{\varphi}^v_{jh}\right)\Big)v_{ih}+\sum_{i=2M+1}^{2M+N}\left(q_{ih},div(\underline{\varphi}^v_{jh})\right)p_{ih}\\
&\qquad-\left(\boldsymbol{\mathcal{A}}_1(\psi_h,c_h),\underline{\varphi}^v_{jh}\right)=\left(\mathbf{F}_u,\underline{\varphi}^u_{jh}+\underline{\varphi}^v_{jh}\right),\qquad\text{for all } 1\le j\le M,
\end{aligned}$$

$$-\sum_{i=2M+1}^{2M+N}\left\{\left(div(\underline{\varphi}^u_{ih}),q_{jh}\right)u_{ih}+\left(div(\underline{\varphi}^v_{ih}),q_{jh}\right)v_{ih}\right\}=0,\quad 2M+1\le j\le 2M+N,$$

$$\begin{aligned}
&\sum_{i=2M+N+1}^{2M+N+\tilde{M}}(z_{ih},z_{jh})\frac{d\psi_{ih}}{dt}+\sum_{i=2M+N+1}^{2M+N+\tilde{M}}\Big\{b_\psi\left(\mathbf{u}_h,z_{ih},z_{jh}\right)+\left(\mathcal{A}_g(\nabla\psi_h)\nabla z_{ih},\nabla z_{jh}\right)\Big\}\psi_{ih}\\
&\qquad+\left(A_2\left(\psi_h,c_h\right),z_{jh}\right)=\left(F_\psi,z_{jh}\right),\quad\text{for all } 2M+N+1\le j\le 2M+N+\tilde{M},
\end{aligned}$$

$$\begin{aligned}
&\sum_{i=2M+N+\tilde{M}+1}^{2M+N+2\tilde{M}}(z_{ih},z_{jh})\frac{dc_{ih}}{dt}+\sum_{i=2M+N+\tilde{M}+1}^{2M+N+2\tilde{M}}\Big\{b_c\left(\mathbf{u}_h,z_{ih},z_{jh}\right)\\
&\qquad+\left(D(\psi_h)\nabla z_{ih},\nabla z_{jh}\right)\Big\}c_{ih}+\sum_{i=2M+N+1}^{2M+N+\tilde{M}}\left(A_3(\psi_h,c_h)\nabla z_{ih},\nabla z_{jh}\right)\psi_{ih}\\
&\qquad=\left(F_c,z_{jh}\right),\quad\text{for all } 2M+N+\tilde{M}+1\le j\le 2M+N+2\tilde{M}.
\end{aligned}$$

The above equations can be written in the differential-algebraic system form (DAE) as

$$\begin{aligned}
&\mathbb{M}\,\frac{d\mathbf{Y}^h}{dt}+\mathbb{A}(\mathbf{Y}^h)\mathbf{Y}^h+\mathbf{L}(\mathbf{Y}^h)=\mathbf{R},\qquad\mathbf{Y}^h(t=0)=\mathbf{Y}^h_0,\\
&\mathbf{Y}^h=\begin{pmatrix}\mathbf{u}_{1h}\cdots\mathbf{u}_{Mh}&p_{1h}\cdots p_{Nh}&\psi_{1h}\cdots\psi_{\tilde{M}h}&c_{1h}\cdots c_{\tilde{M}h}\end{pmatrix}^t,
\end{aligned}\tag{4.3}$$

where $\mathbf{R}=\begin{pmatrix}R_1&0&R_3&R_4\end{pmatrix}^t$, $\mathbf{L}(Y_h)=\begin{pmatrix}L_1&0&L_3&0\end{pmatrix}^t$ and, for $K_1=2M+N+2\tilde{M}$ and $K_2=2M+N+2\tilde{M}$

$$\mathbb{M}=\begin{pmatrix}M_{11}&0&0&0\\0&0&0&0\\0&0&M_{33}&0\\0&0&0&M_{44}\end{pmatrix}\in\mathbb{R}^{K_1,K_2},\qquad\mathbb{A}(\mathbf{Y}_h)=\begin{pmatrix}A_{11}&A_{12}&0&0\\A_{21}&0&0&0\\0&0&A_{33}&0\\0&0&A_{43}&A_{44}\end{pmatrix}\in\mathbb{R}^{K_1,K_2},$$

with

$$
\begin{aligned}
(M_{11})_{ji} &= \rho_0\left(\underline{\varphi}^u_{ih},\underline{\varphi}^u_{jh}\right)+\rho_0\left(\underline{\varphi}^v_{ih},\underline{\varphi}^v_{jh}\right), \quad (M_{33})_{ji}=(z_{ih},z_{jh}), \quad (M_{44})_{ji}=(z_{ih},z_{jh}),\\
(A_{11})_{ji} &= a_u\left(\underline{\varphi}^u_{ih},\underline{\varphi}^u_{jh}\right)+a_u\left(\underline{\varphi}^v_{ih},\underline{\varphi}^v_{jh}\right)+b_u\left(\mathbf{u}_h,\underline{\varphi}^u_{ih},\underline{\varphi}^u_{jh}\right)+b_u\left(\mathbf{u}_h,\underline{\varphi}^v_{ih},\underline{\varphi}^v_{jh}\right)\\
&\quad -\left(b(\psi_h)((\underline{\varphi}^u_{ih}\times\mathbf{B})\times\mathbf{B}),\underline{\varphi}^u_{jh}\right)-\left(b(\psi_h)((\underline{\varphi}^v_{ih}\times\mathbf{B})\times\mathbf{B}),\underline{\varphi}^v_{jh}\right),\\
(A_{12})_{ji} &= \left(q_{ih},\nabla\cdot(\underline{\varphi}^u_{jh})\right)+\left(q_{ih},\nabla\cdot\underline{\varphi}^v_{jh}\right)=(A_{21})_{ij},\\
(A_{33})_{ji} &= (\mathcal{A}_g(\nabla\psi_h)\nabla z_{ih},\nabla z_{jh})+b_\psi\left(\mathbf{u}_h,z_{ih},z_{jh}\right),\\
(A_{43})_{ji} &= (\mathcal{A}_2(\psi_h,c_h)\nabla z_{ih},\nabla z_{jh}), \qquad (A_{44})_{ji}=(D(\psi_h)\nabla z_{ih},\nabla z_{jh})+b_c\left(\mathbf{u}_h,z_{ih},z_{jh}\right),\\
(L_1)_j &= \left(\boldsymbol{\mathcal{A}}_1(\psi_h,c_h),\underline{\varphi}^u_{jh}\right)+\left(\boldsymbol{\mathcal{A}}_1(\psi_h,c_h),\underline{\varphi}^v_{jh}\right), \qquad (L_3)_j=\epsilon_1\left(\mathcal{A}_2(\psi_h,c_h),z_{jh}\right),\\
(R_1)_j &= \left(\mathbf{F}_u,\underline{\varphi}^u_{jh}\right)+\left(\mathbf{F}_u,\underline{\varphi}^v_{jh}\right), \quad (R_3)_j=(F_\psi,z_{jh}), \quad (R_4)_j=(F_c,z_{jh}).
\end{aligned}
\tag{4.4}
$$

The equation (4.3) can be written in general form as

$$
\mathcal{F}(t,\mathbf{Y}^h(t),\frac{d\mathbf{Y}^h}{dt})=0, \qquad \mathbf{Y}^h(t=0)=\mathbf{Y}^h_0. \tag{4.5}
$$

In order to consider the fully discrete scheme, for an integer $K>0$, we introduce the timestep $\tau=\frac{T}{K}$, the time subdivision $t_i=i\tau$ $(0\le i\le K)$ of $[0,T]$ and, for sufficiently regular function $\mathbf{v}$, we denote by $\mathbf{v}_i$ the value of $\mathbf{v}$ at time t_i and by $\partial_{\tau,n}\mathbf{v}=\frac{\mathbf{v}_{n+1}-\mathbf{v}_n}{\tau}$.

The differential-algebraic system (4.3) is first fully discretized by invoking Euler's backward difference method as

$$
\mathcal{F}(t_{n+1},\mathbf{Y}^h_{n+1},\partial_{\tau,n}\mathbf{Y}^h)=0 \tag{4.6}
$$

and then resolved by using the Newton iteration technique on the resulting non-linear fixed-point system, whereas we have made use of the solver DASSL [11].

Then, the following a priori error estimates for the solution (Ψ_h,p_h), with $\Psi_h=(\mathbf{u}_h,\psi_h,c_h)$, of the finite element discretiszation (4.6) can be obtained by adapting similar argument and technique as those in e.g. [2, 24] (for some $\beta_1,\beta_2>1$ and $\alpha\ge 1$)

$$
\|\Psi_h-\Psi\|_{\ell^2(0,T,L^2(\Omega))}\le C_\delta(\tau^\alpha+h^{\beta_1}) \text{ and } \|p_h-p\|_{\ell^2(0,T,L^2(\Omega))}\le C_\delta(\tau^\alpha+h^{\beta_2}) \tag{4.7}
$$

where $C_\delta>0$ is independent of h, $\Psi=(\mathbf{u},\psi,c)$ is the known exact solution of the problem under consideration and the space $\ell^p(0,T,\mathbb{X})$, for a Banach space $\mathbb{X}$ and $0<p<+\infty$ is defined by

$$
\ell^p(0,T,\mathbb{X})=\Big\{\mathbf{v}:(t_1,...,t_k)\to\mathbb{X} \text{ such that } \|\mathbf{v}\|_{\ell^p(0,T,\mathbb{X})}=\left(\tau\sum_{i=1}^{k}\|\mathbf{v}_i\|^p_{\mathbb{X}}\right)^{1/p}<\infty\Big\}.
$$

Note that β_i, $i=1,2$, are greater than 1 and less than minimum of the degree of the finite elements (polynomials) and the Sobolev space regularity of the solutions. Moreover, for optimal spatial (resp. temporal) convergence rate we take $\tau^\alpha\le h^{\beta_i}$, $i=1,2$ (resp. $h^{\beta_i}\le\tau^\alpha$, $i=1,2$).

Remark 4.1 *The constant C_δ is independent of h but depends, among other things, on the solution and in particular on the interface thickness δ, which is a "worst-case" error estimate for phase field model (see e.g., [6])*

In the next section, we validate the convergence results (4.7) and the stability of numerical scheme by numerical experiments.

5 Analysis of the numerical scheme

In this section, we present numerical examples to verify theoretical estimates (4.7) and stability of the method. To investigate the convergence rates of the numerical scheme, two numerical tests are conducted:

the first evaluates the time discretization error, and the second evaluates the spatial discretization error. In order to ascertain the numerical stability of the method, we include $(1 - \epsilon\ randf)$ in the artificial source terms to introduce ϵ-perturbations in the numerical solution, where random function *randf* (which generates some F-distributed random variables) assumes values in $[0, 1]$ and ϵ is the perturbation control parameter. The values of the physical parameters are consistent with that given in [29] and the constants for the meltflow equations are chosen in accordance with the physical properties of the nickelcopper (NiCu) system see Table 1 (see e.g., [18]).

Property Name	Symbol	Unit	Nickel (A)	Copper (B)
Melting temperature	T_m	K	1728	1358
Latent heat	L	J/m^3	2350×10^6	1758×10^6
Diffusion coeff. liquid	D_L	m^2/s	10^{-9}	10^{-9}
Diffusion coeff. solid	D_S	m^2/s	10^{-13}	10^{-13}
Linear kinetic coeff.	β	$m/K/s$	3.3×10^{-3}	3.9×10^{-3}
Interface thickness	δ	m	8.4852×10^{-8}	6.0120×10^{-8}
Density	ρ	Kg/m^3	7810	8020
viscosity	μ	$Pa \cdot s$	4.110×10^{-6}	0.597×10^{-6}
Surface energy	σ	J/m^2	0.37	0.29
Electrical conductivity	σ_e	S/m	14.3×10^6	59.6×10^6
Molar volume	V_m	m^3	7.46×10^{-6}	7.46×10^{-6}
Mode Number	k	N/A	4	4
Anisotropy Amplitude	γ_0	N/A	0.04	0.04

Table 1: Physical values of constants

As exact solutions, we consider the two following examples (with $T = 1$ and $\mathbf{B} = \frac{1}{\sqrt{2}}(1, 1)$).

- Example 1 :

$$\begin{aligned} u_{ex}(x,y,t) &= \frac{2}{(2\pi)^2} e^{1-t} sin(x)^2 y(1-\frac{y}{2\pi})(1-\frac{y}{\pi}), \\ v_{ex}(x,y,t) &= -\frac{2}{(2\pi)^2} e^{1-t} sin(x)cos(x)y^2(1-\frac{y}{2\pi})^2, \quad p_{ex}(x,y,t) = e^{1-t}cos(y), \\ \psi_{ex}(x,y,t) &= \frac{e^{1-t}}{2}(cos(x)cos(y)+1), \quad c_{ex}(x,y,t) = \frac{8}{(2\pi)^2} e^{1-t} x^2 (1-\frac{x}{2\pi})^2(cos(y)+1), \end{aligned} \tag{5.1}$$

  where $\Omega = [0, 2\pi] \times [0, 2\pi]$.

- Example 2 :

$$\begin{aligned} u_{ex}(x,y,t) &= 4\pi e^{t-1} x^2(1-x)^2 sin(2\pi y)cos(2\pi y), \\ v_{ex}(x,y,t) &= -2e^{t-1}x(2x^2-3x+1)sin^2(2\pi y), \quad p_{ex}(x,y,t) = e^{t-1}cos(2\pi x), \\ \psi_{ex}(x,y,t) &= \frac{1}{4}e^{t-1}(cos(2\pi x)+cos(2\pi y)+2), \quad c_{ex}(x,y,t) = 8e^{t-1}(x^2(1-x)^2+y^2(1-y)^2), \end{aligned} \tag{5.2}$$

  where $\Omega = [0, 1] \times [0, 1]$.

The right-hand side terms $\mathbf{F}_u$, F_ψ and F_c are computed appropriately to ensure that (5.1) (resp. (5.2)) is the exact solution of system (2.1). Furthermore, we consider a sequence of four meshes with a decreasing step h (see Fig.1 and Table 2).

5.1 Numerical error analysis

To numerically verify the error estimates and the convergence orders of scheme, two types of computations have been made. First, we have estimated the spatial convergence rates wherein sufficiently small timesteps τ (as compared to the spatial step size h) are fixed and we have varied the spatial step size h as described in

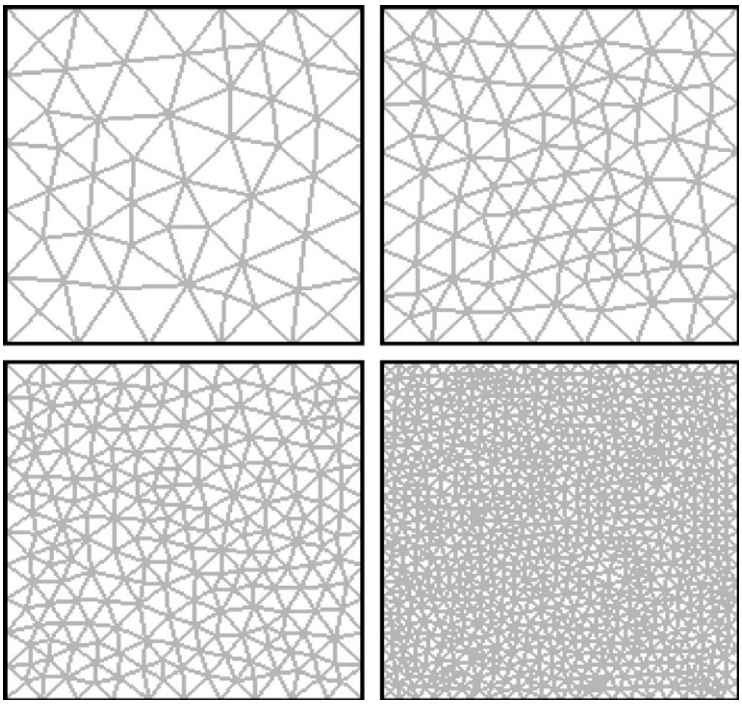

Figure 1: Meshes

Mesh	h	Elements	Boundary elements
1	0.2	106	5
2	0.15	200	7
3	0.1	434	10
4	0.05	1712	20

Table 2: Mesh Statistics

Table 2 of mesh statistics. In order to calculate the rates β_1 and β_2 with respect to h, we use the Lagrange-quadratic $\mathbb{P}_2$ and Lagrange-cubic $\mathbb{P}_3$ finite elements for the phase-field and concentration system, and the velocity/pressure mixed finite elements $\mathbb{P}_2 - \mathbb{P}_1$ and $\mathbb{P}_3 - \mathbb{P}_2$ for the flow system.

In Fig. 2 and Fig. 3, $L^2(\mathcal{Q})$-norms of errors of $\mathbf{u}$, p, ψ and c are plotted versus h and τ respectively, in *log*-scales. For h-curves, we use $\tau = 0.01$, $\tau = 0.001$ and $\tau = 0.0001$ for linear, quadratic and cubic finite elements, respectively. It is observed that the slopes of error curves for the velocity, phase-field and concentration are approximately equal to 3 and 4 for quadratic and cubic finite elements respectively, whereas the slopes of error curves for the pressure are approximately equal to 2 and 3 for linear and quadratic finite elements respectively; refer to Table 3 and Table 4. τ-curves slopes of all the curves are approximately 1, i.e., $\alpha = 1$; refer to Table 5 and Table 6. Both of these numerical estimates are in good agreement with the postulated error estimate (4.7).

5.2 Numerical stability analysis

In order to study the stability of the method, we include $(1 - \epsilon\ randf)$ in the artificial source terms to introduce ϵ-perturbations in the numerical solution, where the random function *randf* assumes values in $[0, 1]$ (see e.g. Fig. 4) and ϵ is the perturbation control parameter. We fix $h = 0.2$ and $\tau = 0.1$ and we use quadratic finite elements $\mathbb{P}_2$ for ψ, c and $\mathbf{u}$ and linear finite elements $\mathbb{P}_1$ for p. We perform three different computational stability tests (in Fig.5, Fig.6, Fig.7 and Fig.8).

	Error Estimate	$\mathbf{P}_2 - \mathbf{P}_1$	$\mathbf{P}_3 - \mathbf{P}_2$
Example 1	β_1 for $\mathbf{u}$	2.6201	3.8730
	β_2 for p	1.9207	3.0646
Example 2	β_1 for $\mathbf{u}$	2.7664	4.0303
	β_2 for p	2.3462	3.4302

Table 3: Order of convergence β_i, $(i = 1, 2)$, for velocity $\mathbf{u}$ and pressure p in Examples 1 and 2.

	Error Estimate	$\mathbf{P}_2$	$\mathbf{P}_3$
Example 1	β_1 for ψ	2.7001	3.7500
	β_1 for c	2.9278	3.8739
Example 2	β_1 for ψ	2.9200	3.8200
	β_1 for c	2.8972	4.0681

Table 4: Order of convergence β_1 for phase-field ψ and concentration c in Examples 1 and 2.

In Fig. 5, the $L^2(\mathcal{Q})$-norm of the discrepancy between exact solution $\Phi_{ex} = (\Phi_{ex}^{(s)})_{s=1,4} = (\mathbf{u}_{ex}, p_{ex}, \psi_{ex}, c_{ex})$ and its ϵ-perturbation $\Phi_\epsilon = (\Phi_\epsilon^{(s)})_{s=1,4} = (\mathbf{u}_\epsilon, p_\epsilon, \psi_\epsilon, c_\epsilon)$ i.e. $E_{\epsilon,ex}\left(\Phi_\epsilon^{(s)} - \Phi_{ex}^{(s)}\right) = \left\|\Phi_\epsilon^{(s)} - \Phi_{ex}^{(s)}\right\|_{L_2(Q)}$, for $s = 1, 4$ are plotted versus ϵ (which are shown for $\epsilon = 0.01, 0.05, 0.1, 0.15, 0.2, 0.3, 0.4$). A linear dependence

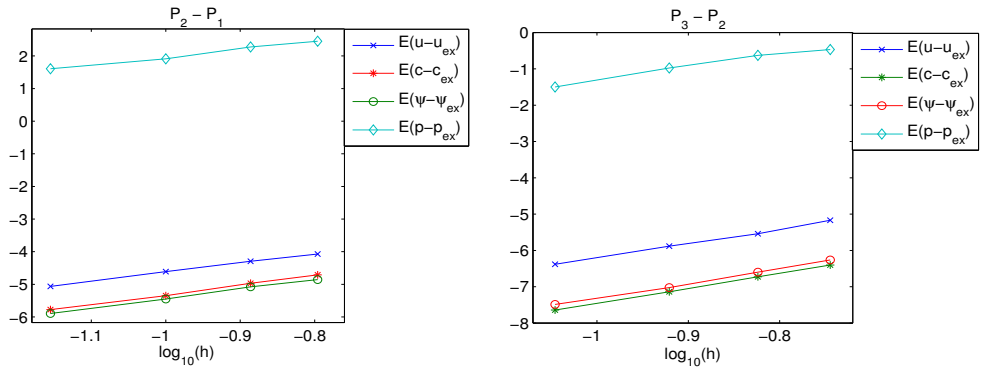

(a) Spatial error curves in Example 1

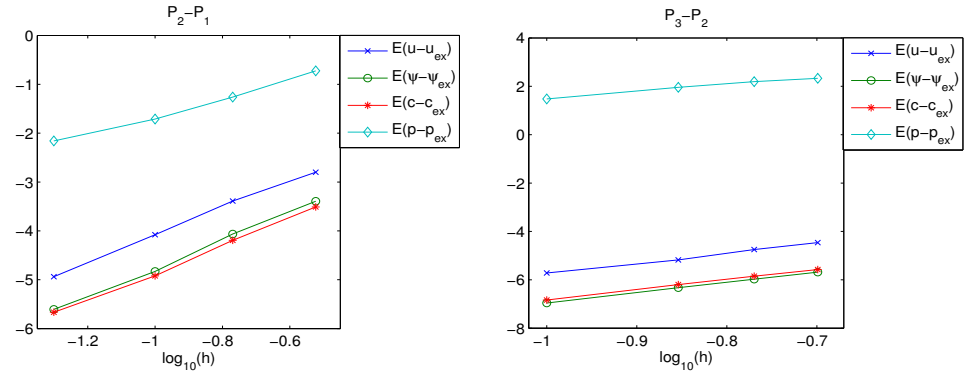

(b) Spatial error curves in Example 2

Figure 2: Error curves with respect to spatial step h obtained in Examples 1 and 2.

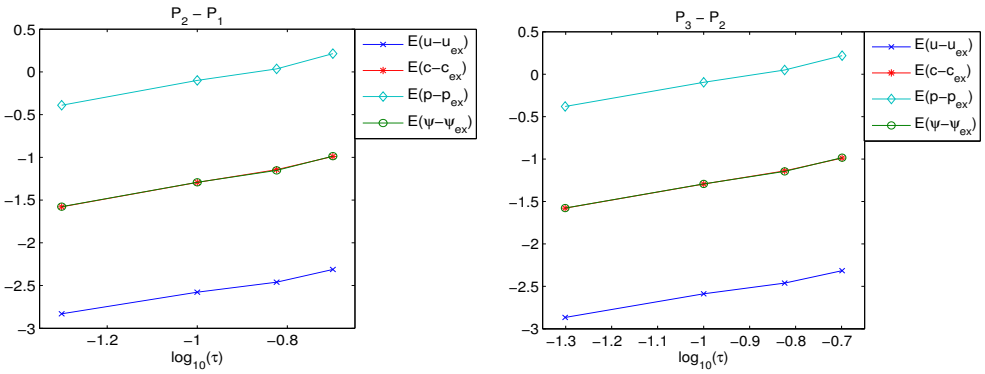

(a) Temporal error curves in Example 1

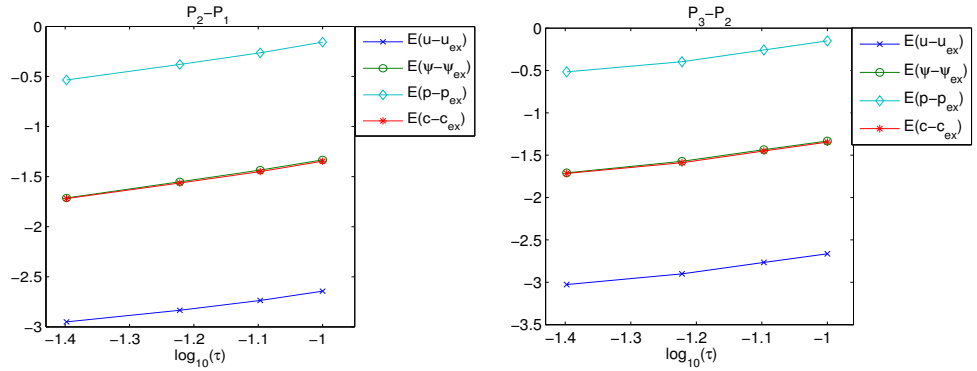

(b) Temporal error curves in Example 2

Figure 3: Error curves with respect to temporal step τ obtained in Examples 1 and 2.

	Error Estimate	$\mathbf{P}_2 - \mathbf{P}_1$	$\mathbf{P}_3 - \mathbf{P}_2$
Example 1	α for $\mathbf{u}$	1.1494	1.1446
	α for p	1.0733	1.0634
Example 2	α for $\mathbf{u}$	0.9011	0.9152
	α for p	1.0032	0.9944

Table 5: Order of convergence α for velocity $\mathbf{u}$ and pressure p in Examples 1 and 2.

	Error Estimate	$\mathbf{P}_2$	$\mathbf{P}_3$
Example 1	α for ψ	1.0558	1.0396
	α for c	1.0602	1.0565
Example 2	α for ψ	0.9821	0.9856
	α for c	0.9792	0.9815

Table 6: Order of convergence α for phase-field ψ and concentration c in Examples 1 and 2.

of errors on ϵ is observed, indeed, $E_{\epsilon,ex}\left(\Phi_{\epsilon}^{(s)} - \Phi_{ex}^{(s)}\right) \approx m_s\ \epsilon$, for $s = 1, 4$, where m_s represents the slope of the error curve; refer to Table 7. In Fig. 6, the error $E_{\epsilon,app}\left(\Phi_{\epsilon}^{(s)} - \Phi_{app}^{(s)}\right) = \left\|\Phi_{\epsilon}^{(s)} - \Phi_{app}^{(s)}\right\|_{L_2(Q)}$, for $s = 1, 4$ between the approximate solution $\Phi_{app} = (\Phi_{app}^{(s)})_{s=1,4} = (\mathbf{u}_{app}, p_{app}, \psi_{app}, c_{app})$ without random

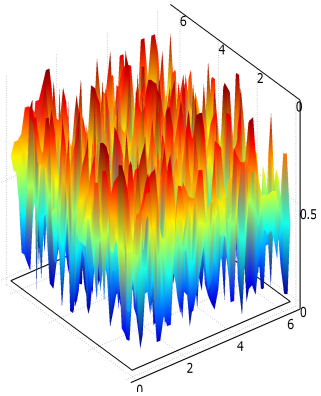

Figure 4: Random function.

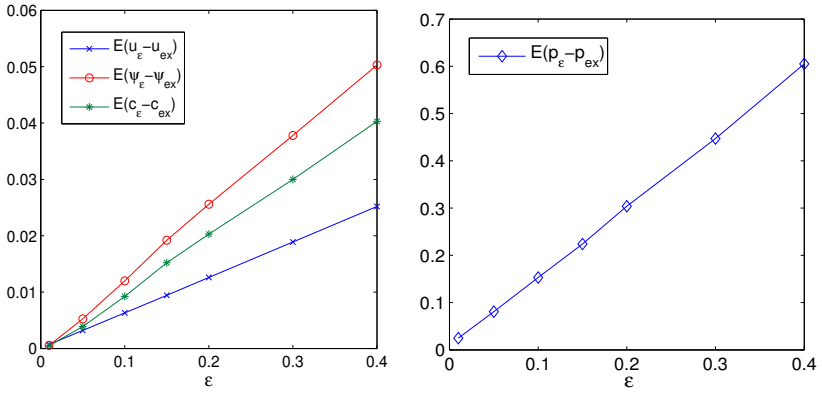

(a) Error curves in Example 1

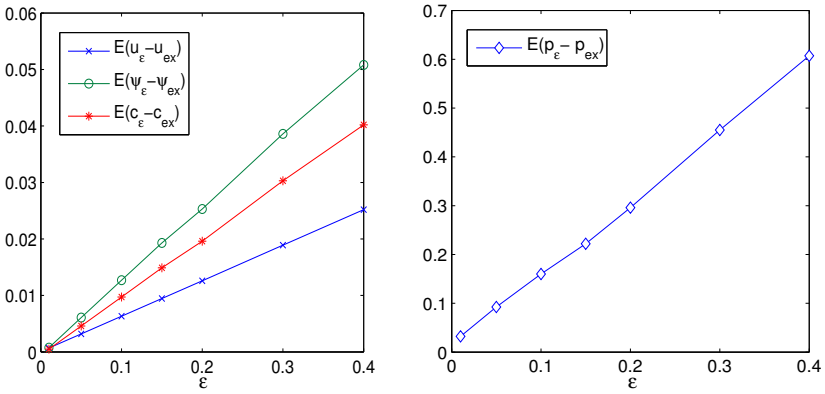

(b) Error curves in Example 2

Figure 5: Errors Curves of norm $EE_{\epsilon,ex}$.

(i.e., $\epsilon = 0$) and Φ_ϵ, are plotted against ϵ. The same observation holds as in Fig. 5; refer also to Table 7.

Finally, in Fig. 7 and Fig. 8, the solution curves for different perturbation levels are delineated on a part of the domain and at time $t = 1$ in order to establish stability with respect to random perturbations. In Fig. 7, we fix $y = \pi/2$ and x varies for velocity and concentration, and $t = 1$, $x = \pi$ and y varies for

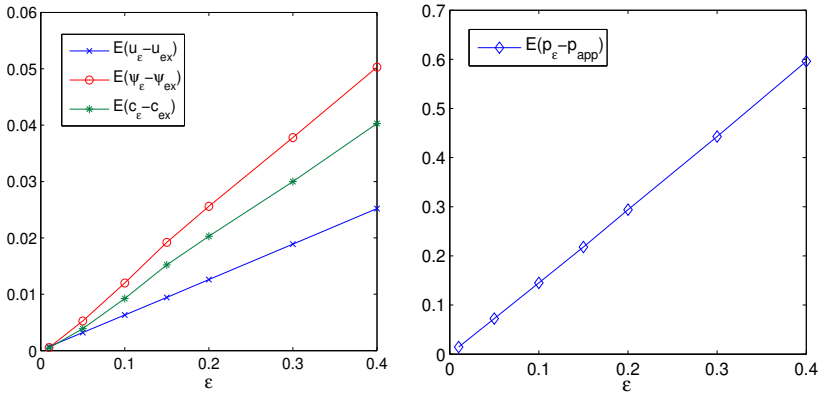

(a) Error curves in Example 1

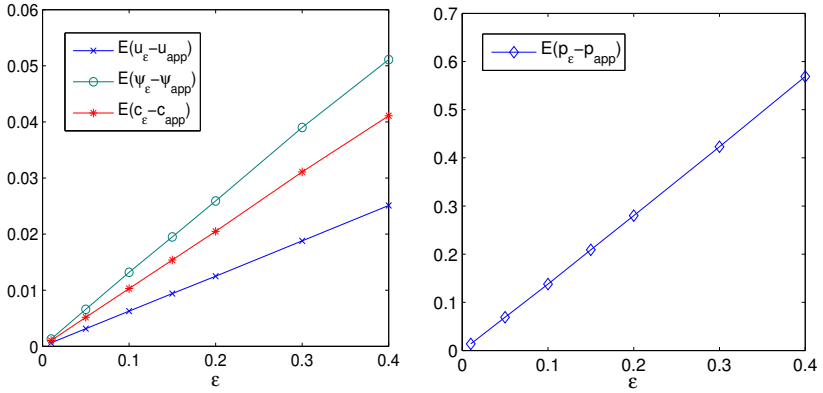

(b) Error curves in Example 2

Figure 6: Errors Curves of norm $E_{\epsilon,app}$.

pressure and phase field. In Fig. 8 we fix $x = 1/2$ and y varies for velocity and phase field, and $x = 1/2$ and y varies for pressure and concentration. The graphs substantiate that the solution is indeed stable (and it does not become unstable by increasing the random error).

	Slope	$E_{\epsilon,ex}$	$E_{\epsilon,app}$
Example 1	$m_{\mathbf{u}}$	0.1701	0.1754
	m_{ψ}	0.8638	0.8818
	m_c	0.4341	0.4371
	m_p	1.4738	1.4913
Example 2	$m_{\mathbf{u}}$	0.0628	0.0635
	m_{ψ}	0.1283	0.1347
	m_c	0.1018	0.1065
	m_p	1.4877	1.4236

Table 7: Slopes of Norm L_2 in Examples 1 and 2.

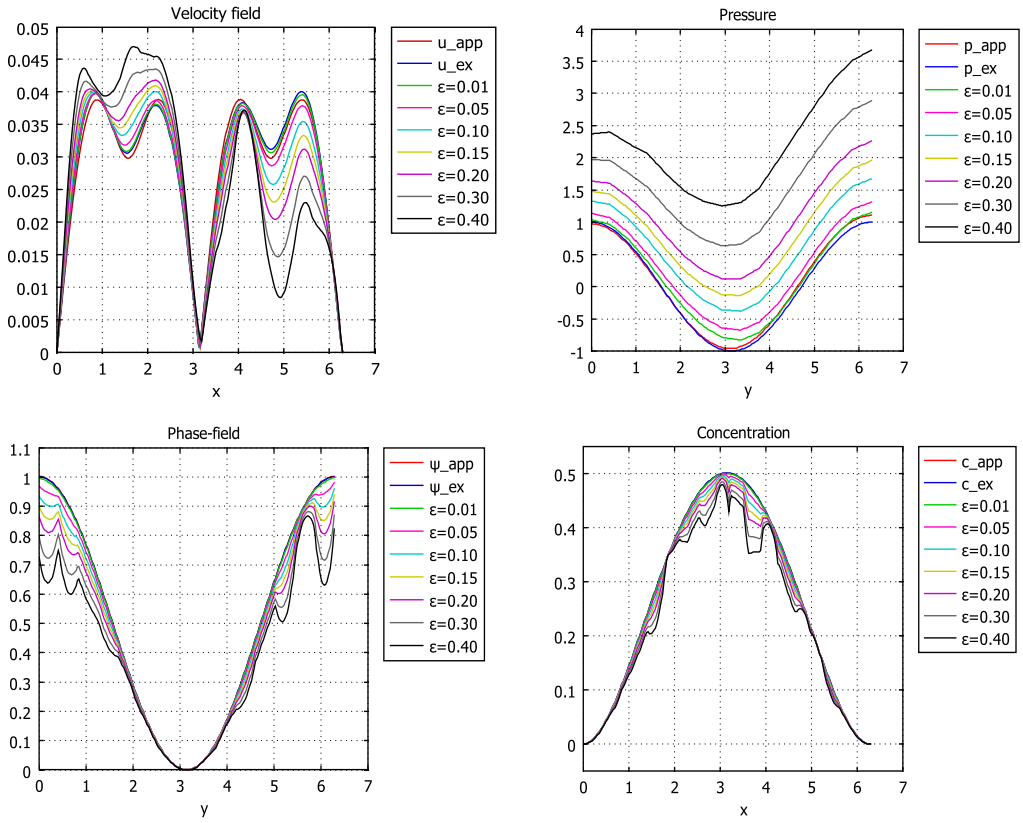

Figure 7: Solution curves for the different values of ϵ in Example 2.

6 A physical test

In this section we present realistic numerical simulations of dendrite growth during the solidification process of the binary mixture of Nickel-Copper (Ni-Cu). We present first the non-dimensionalization of the model (2.1) (there is no artificial forcing terms) and the details of the physical parameters used in the numerical simulations. In order to nondimensionalize (2.1) we introduce the following dimensionless quantities

$$\tilde{\mathbf{x}} = \frac{\mathbf{x}}{\ell}, \quad \tilde{t} = \frac{D_L t}{\ell^2}, \quad \tilde{\mathbf{u}}(\tilde{\mathbf{x}}, \tilde{t}) = \frac{\ell}{D_L}\mathbf{u}(\mathbf{x}, t), \quad \tilde{p} = \frac{\ell^3}{\rho_0 D_L^2} p$$
$$\tilde{\mathbf{B}} = \frac{\mathbf{B}}{B_0}, \quad \tilde{\psi}(\tilde{\mathbf{x}}, \tilde{t}) = \psi(\mathbf{x}, t), \quad \tilde{c}(\tilde{\mathbf{x}}, \tilde{t}) = c(\mathbf{x}, t),$$

where $\tilde{\mathbf{x}}$ and $\tilde{t}$ are the dimensionless spatial and time coordinates, $\tilde{\mathbf{u}}$, $\tilde{\psi}$, and $\tilde{c}$ are the nondimensional velocity-field, phase-field and concentration respectively, D_L is the solutal diffusivity in liquid, ℓ is the characteristic length of the domain Ω, ℓ^2/D_L is the liquid diffusion time and B_0 is the characteristic magnetic-field. Note that the phase-field is a mathematical quantity and c is the relative concentration which are already dimensionless quantities. Using these adimensional relations, we get finally the dimen-

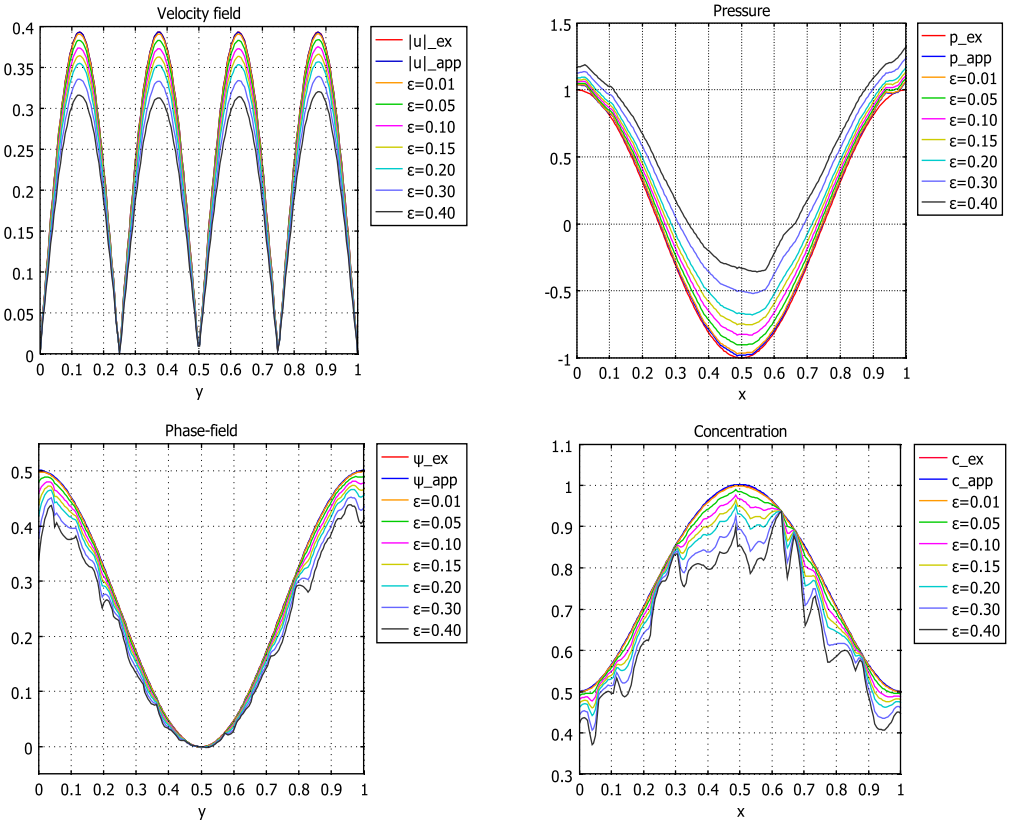

Figure 8: Solution curves for the different values of ϵ in Example 1.

sionless system

$$\begin{aligned}
&\frac{\partial \tilde{\mathbf{u}}}{\partial \tilde{t}} + (\tilde{\mathbf{u}}.\tilde{\nabla})\tilde{\mathbf{u}} = -\tilde{\nabla}\tilde{p} + \tilde{\mu}\tilde{\Delta}\tilde{\mathbf{u}} + \tilde{\boldsymbol{\mathcal{A}}}_1(\tilde{\psi},\tilde{c}) + \tilde{b}(\tilde{\psi})(\tilde{\mathbf{u}}\times\tilde{\mathbf{B}})\times\tilde{\mathbf{B}} \quad \text{on} \quad \tilde{\mathcal{Q}} = \tilde{\Omega}\times(0,\tilde{T}),\\
&\operatorname{div}(\tilde{\mathbf{u}}) = 0 \quad \text{on} \quad \tilde{\mathcal{Q}},\\
&\frac{\partial \tilde{\psi}}{\partial \tilde{t}} + (\tilde{\mathbf{u}}.\tilde{\nabla})\tilde{\psi} = \tilde{\operatorname{div}}\left(\tilde{\mathcal{A}}_g(\tilde{\nabla}\tilde{\psi})\tilde{\nabla}\tilde{\psi}\right) - \tilde{\mathcal{A}}_2(\tilde{\psi},\tilde{c}) \quad \text{on} \quad \tilde{\mathcal{Q}},\\
&\frac{\partial \tilde{c}}{\partial \tilde{t}} + (\tilde{\mathbf{u}}.\tilde{\nabla})\tilde{c} = \tilde{\operatorname{div}}\left(\tilde{D}(\tilde{\psi})\tilde{\nabla}\tilde{c} + \tilde{\mathcal{A}}_3(\tilde{\psi},\tilde{c})\tilde{\nabla}\tilde{\psi}\right) \quad \text{on} \quad \tilde{\mathcal{Q}},
\end{aligned} \tag{6.1}$$

with

$$\begin{aligned}
&\tilde{\mathcal{A}}_g(\tilde{\nabla}\tilde{\psi}) = \frac{1}{D_L}\mathcal{A}_g(\tilde{\nabla}\tilde{\psi}), \quad \tilde{b}(\tilde{\psi}) = Pr(Ha)^2 a_2(\tilde{\psi}),\\
&\tilde{\boldsymbol{\mathcal{A}}}_1(\tilde{\psi},\tilde{c}) = PrRa_c a_1(\tilde{\psi})\tilde{c}\mathbf{e}_G + Kr\mathbf{f}(\tilde{\psi}), \quad \tilde{\mathcal{A}}_2(\tilde{\psi},\tilde{c}) = \tilde{M}_\psi\left(\frac{\lambda_1(\tilde{c})}{\tilde{\delta}^2}g'(\tilde{\psi}) + \frac{\tilde{\lambda}_2(\tilde{c})}{\tilde{\delta}}\bar{p}'(\tilde{\psi})\right),\\
&\tilde{\mathcal{A}}_3(\tilde{\psi},\tilde{c}) = \alpha_0\tilde{D}(\tilde{\psi})\tilde{c}(1-\tilde{c})\left(\frac{\lambda_1'(\tilde{c})}{\delta}g'(\tilde{\psi}) - \tilde{\lambda}_2'(\tilde{c})\bar{p}'(\tilde{\psi})\right),
\end{aligned} \tag{6.2}$$

where $\tilde{\mu} = Pr = \mu/D_L$ is the Prandtl number, $Ra_c = g\beta_c\ell^3/D_L\mu$, is the solutal Rayleigh number, $Ha = (\sigma_e/\rho_0\mu)^{1/2}B_0\ell$ is the Hartmann number and $Kr = \zeta\ell^3/\rho_0 D_L^2$, $\tilde{\delta} = \delta/\ell$ is the adimensional interface thickness, $\tilde{\lambda}_2 = \ell\lambda_2$, $\tilde{\alpha}_0 = \alpha_0/\ell$, $\tilde{M}_\psi = M_\psi/D_L$ and $\epsilon_2 = \tilde{M}_\psi\epsilon_0^2$ are the adimensional parameters and $\mathbf{e}_G = (0,1)$. The density ρ, viscosity μ, and electrical conductivity σ_e are assumed to be constant in the liquid as well as in the solid, therefore we have used average values of Ni and Cu for these constants in the simulations and we define $\zeta = 3.57\ 10^4 kgm^{-2}s^{-2}$ and $B_0 = 10$. The adimensional space unit ℓ is chosen as $\ell = 2.8284\times10^{-6}m$ which gives the domain length equal to 8 and the domain as $\tilde{\Omega} = [-4,4]\times[-4,4]$.

With this value of ℓ, we have the adimensional $\tilde{\delta} = 0.03$ which corresponds to an interface thickness δ of order $10^{-8}m$. Since the value of δ is strongly dependent on the size of mesh and as the mesh size should be sufficiently less than the interface thickness δ and as we have used a coarse mesh for our simulations due to technical difficulties in computations, therefore we fix the value of the adimensional interface thickness as $\tilde{\delta} = 0.05$ for our simulations to ensure the mesh size less than the interface thickness. Moreover we have used some strategies to construct a necessary fixed structured grid to properly resolve the sharp fronts in this dendritic solidification problem (for more details see [18]). The adimensional final time is $\tilde{T} = 0.125$, which corresponds to the real physical final time of $T = 1\ ms$. Note that big time steps and smaller interface values can create convergence problems during the calculation of numerical solution of the problem. We choose the values of the physical parameters (see Table 1) for the phase-field and concentration equations as given in [29] and the parameters associated with the flow system are chosen by keeping in view the properties of substances A (Copper (Cu) in the present case) and B (Nickel (Ni) in the present case).

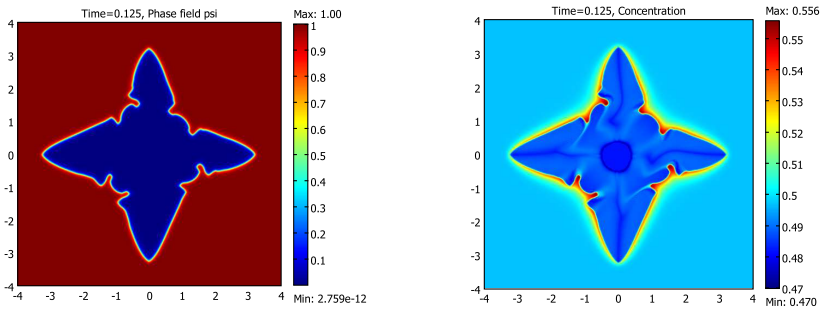

Figure 9: Plots of phase-field and concentration

At initial time the computational domain $\tilde{\Omega}$ is liquid and the solidification starts with an initial circular grain (or seed) of radius $\sqrt{0.2}$ at the center of the domain $\tilde{\Omega}$. The value of $\tilde{\psi}$ inside the grain is 0 otherwise the value of $\tilde{\psi}$ is 1. The concentration $\tilde{c}$ in the initial grain is equal to 0.482 and outside the grain it is taken to be 0.497. The velocity inside and outside the circular seed is taken to be 0 at the start of the solidification. We have solved the model using $\mathbb{P}_3$ for the velocity, phase-field and concentration and $\mathbb{P}_2$ for the pressure.

In Fig. 9, we present the phase-field and concentration with the magnetic-field $\tilde{\mathbf{B}} = \frac{1}{\sqrt{2}}(1,1)$ (at an angle 45°) at final time $\tilde{T}$. In this case, we observe that the dendrite is deformed along the direction of the applied magnetic field (unlike the case of zero magnetic field, where the dendrite is completely symmetric about x-axis and y-axis). More analysis can be found in [18].

7 Concluding remarks

In this paper we have elaborated numerical resolution of the isothermal anisotropic solidification model (2.1) and validated it by performing its error and stability analysis. First, we have discretized the problem with respect to spatial coordinates using mixed finite elements, which satisfy the InfSup condition (Babuska-Brezi's condition), for the velocity $\mathbf{u}$ and pressure p and the usual finite elements for phase-field ψ and concentration c. More precisely we have used mixed finite elements $\mathbb{P}_i - \mathbb{P}_{i-1}$ for the velocity $\tilde{\mathbf{u}}$ and pressure $\tilde{p}$ and $\mathbb{P}_i$ for the phase-field $\tilde{\psi}$ and concentration $\tilde{c}$ respectively, where $\mathbb{P}_i$ is the polynomial of degree i. We obtain a system of nonlinear ordinary differential equations. The derived non-linear systems are then solved by using solver DASSL.

Second, we have studied the convergence (both with respect to space and time variables) and stability of the scheme by considering two examples with known exact solutions (with parameters and data corre-

sponding to the mixture Ni-Cu). We have demonstrated numerically that the error estimates with respect to space are of order $i+1$ for $\mathbf{u}$, ψ and c and of order i for p, and the error estimates with respect to time are of order 1 for $(\mathbf{u}, p, \psi, c)$. Both of these numerical estimates are in good agreement with the postulated error estimate defined in (4.7). The stability of the scheme has also been studied by introducing a random function, which varies between 0 and 1, in the model. We found that the numerical scheme is stable and it has linear dependence with the increase in percentage error. The simulations can be broaden for the non-isothermal anisotropic case by the inclusion of the temperature equation.

References

[1] Anderson D. M., McFadden G. B., Wheeler A. A., "A phase-field model of solidification with convection", *Physica D*, Vol. **135**, pp. 175-194, 2000. 1

[2] Belmiloudi A., "Method of characteristics and error estimates of the perturbation of given mean flow. Application of mathematics in Engineering and Business Sozopol", *Proceedings of the XXII Summer School*, pp. 25-38, 1996. 7

[3] Belmiloudi A., " Robin-type boundary control problems for the nonlinear Boussinesq type equations", *Journal of Mathematical Analysis & Applications*, Vol. **273**, pp. 428-456, 2002. 3, 4

[4] Belmiloudi A., " Robust and optimal control problems to a phase-field model for the solidification of a binary alloy with a constant temperature", *Journal of Dynamical & Control Systems*, Vol. **10**, pp. 453-499, 2004. 1

[5] Belmiloudi A., "Stabilization, optimal and robust control: Theory and Applications in Biological and Physical Systems", Springer-Verlag, London, Berlin, 2008. 1

[6] Chen Z., Hoffmann K. H., " An error estimate for a finite-element scheme for a phase field model", *IMA J. Numer. Anal.*, Vol. **14**, pp. 243255, 1994. 7

[7] Galindo V., Gerbeth G., Ammon W. V., Tomzig E., Virbulis J., "Crystal growth melt flow previous term control next term by means of magnetic fields", *Energy Conv. Manage.* Vol. **43**, pp. 309-316, 2002. 1

[8] Grujicic M., Cao G., Millar R. S., "Computer modelling of the evolution of dendrite microstructure in binary alloys during non-isotheraml solidification", *J. Materials synthesis and processing*, Vol. 10, No. 4, 191-203, 2002. 1

[9] Gunzberger M., Ozugurlu E., Turner J., Zhang H., "Controlling transport phenomena in the Czochralski crystal growth process", *J. Crystal Growth*, Vol. **234**, pp. 47-62, 2002. 1

[10] Hadid H. B., Henry D., Kaddeche S., "Numerical study of convection in the horizontal Bridgman configuration under the action of a constant magnetic field. Part 1. Two dimensional flow", *J. Fluid Mech.*, Vol. **333**, pp. 23-56, 1997. 1

[11] Petzold L. R., "A discription of DASSL: A differential/algebraic system solver", *Scientific computing, IMACS Trans. Sci. Comput.*, pp. 65-68, 1983. 7

[12] Li M., Takuya T., Omura N., Miwa K., "Effects of magnetic field and electric current on the solidification of AZ91D magnesium alloys using an electromagnetic vibration technique", *J. of Alloys and Compounds*, Vol. **487**, pp. 187-193, 2009. 1

[13] Ramizer J. C., Beckermann C., Kerma A., Diepers H. J., "Phase-field modeling of binary alloy solidification with couple heat and solute diffusion", *Physical Review E*, Vol **69**, pp. (051607-1)-(051607-16), 2004. 1

[14] Ramizer J. C., Beckermann C., "Examination of binary alloy free dendritic growth theories with a phase-field model", *Acta Materialia*, Vol. **53**, pp. 1721-1736, 2005. 1

[15] Rappaz M., Rettenmayr M., "Simulation of solidification", *Current Opinion in Solid State and Materials Science*, Vol. **3**, pp. 275-282, 1998. 1

[16] Rasheed A., Belmiloudi A., Mahe F., "Dynamics of dendrite growth in a binary alloy with magnetic field affect", *Discrete and Continuous Dynamical Systems*, Vol. **2011**, pp. 1224-1233, Special Issue, 2011. 1

[17] Rasheed A., Belmiloudi A., "An analysis of the Phase-field model for isothermal binary alloy solidification with convection under the influence of magnetic field", *Journal of Mathematical Analysis & Applications*, Vol. **390**, pp. 244-273, 2012. 1

[18] Rasheed A., Belmiloudi A., "Mathematical Modelling and Numerical Simulation of Dendrite Growth Using Phase-Field Method with a Magnetic Field Effect", *Communications in Computational Physics*, Vol. **14**, pp. 477-508, 2013. 1, 2, 3, 8, 16

[19] Rasheed A., Wahab, A., "Numerical analysis of an isotropic phase-field model with magnetic-field effect", *C.R. Acad. Sci. Paris, Ser. I*, Vol. **353**, pp. 219-224, 2015. 2

[20] Rasheed A., Belmiloudi A., "Phase-field method for computationally efficient modeling of the solidification of binary alloy with magnetic field effect", In. Proceedings of the NumAn2010 Conference in Numerical Analysis; Recent Approaches to Numerical Analysis: Theory, Methods and Applications, (eds., V. Dougalis, E. Gallopoulos, A. Hadjidimos et al.), pp. 222-230, 2010. 1

[21] Roplekar J. K., Dantzig J. A., "A study of solidification with a rotating magnetic field", *Int. J. Cast Met. Res.* Vol. **14**, pp. 79-95, 2001. 1

[22] Prescott P. J., Incropera F. P., "Magnetically damped convection during solidification of a binary metal alloy", *Trans. ASME*, Vol. **115**, pp. 302-310, 1993. 1

[23] Sampath R., "The adjoint method for the design of directional binary alloy solidification processes in the presence of a strong magnetic field", Thesis, Cornell University USA, 2001. 1

[24] Süli E., "Convergence and non-linear stability of Lagrange-Galerkin method for the Navier-Stokes equations.", *Numer. Math*, Vol. **53**, pp. 459-483, 1988. 7

[25] Takaki T., Fukuoka T., Tomita Y., "Phase-field Simulations during Directional Solidification of a Binary Alloy using Adaptive Finite Element Method", *J. Crystal Growth*, Vol. **283**, pp. 263-278, 2005. 1

[26] Temam,R., "NavierStokes Equations", North-Holland, Amsterdam, 1977. 4

[27] Tonhardt R., Amberg G., "Simulation of natural convection effects on succinonitrile crystals", *Physical Review E*, Vol. **62**, No. 1, pp. 828-836, 2000. 1

[28] Tong X., Beckermann C., Kerma A., Li Q., "Phase-field simulations of dendritic crystal growth in a forced flow", *Physical Review E*, Vol **63**, pp. (061601-1)-(061601-16), 2001. 1

[29] Warren J. A., Boettinger W. J., "Prediction of dendritic growth and microsegregation patterns in a binary alloy using the phase-field method", *Acta metall. mater*, Vol. 43, No. 2, pp. 689-703, 1995. 1, 2, 8, 16

[30] Watanabe M., Vizman D., Friedrich J., Mueller G., "Large modification of crystal-melt interface shape during Si crystal growth by using electromagnetic Czochralski method", *J. Crystal Growth*, Vol. **292**, pp. 252-256, 2006. 1